pH- and thermo-sensitive MTX-loaded magnetic nanocomposites: synthesis, characterization, and *in vitro* studies on A549 lung cancer cell and MR imaging

Masoud Farshbaf, Roya Salehi, Nasim Annabi, Rovshan Khalilov, Abolfazl Akbarzadeh & Soodabeh Davaran

Taylor & Francis
Taylor & Francis Group

Check for updates

RESEARCH ARTICLE

pH- and thermo-sensitive MTX-loaded magnetic nanocomposites: synthesis, characterization, and *in vitro* studies on A549 lung cancer cell and MR imaging

Masoud Farshbaf[a,b,c], Roya Salehi[b], Nasim Annabi[d,e,f], Rovshan Khalilov[g,h], Abolfazl Akbarzadeh[c,i,j] and Soodabeh Davaran[k]

[a]Department of Medical Nanotechnology, Faculty of Advanced Medical Sciences, Tabriz University of Medical Sciences, Tabriz, Iran; [b]Drug Applied Research Center and Department of Medical Nanotechnology, Faculty of Advanced Medical Sciences, Tabriz University of Medical Sciences, Tabriz, Iran; [c]National Institute for Medical Research Development (Nimad), Tehran, Iran; [d]Biomaterials Innovation Research Center, Brigham and Women's Hospital, Harvard Medical School, Cambridge, MA, USA; [e]Harvard-MIT Division of Health Sciences and Technology, Massachusetts Institute of Technology, Cambridge, MA, USA; [f]Department of Chemical Engineering, Northeastern University, Boston, MA, USA; [g]Institute of Radiation Problems, National Academy of Sciences of Azerbaijan, Baku, Azerbaijan; [h]Joint Ukrainian-Azerbaijan International Research and Education Center of Nanobiotechnology and Functional Nanosystems, Baku, Azerbaijan; [i]Stem Cell Research Center, Tabriz University of Medical Sciences, Tabriz, Iran; [j]Universal Scientific Education and Research Network (USERN), Tabriz, Iran; [k]Research Center for Pharmaceutical Nanotechnology, Tabriz University of Medical Sciences, Tabriz, Iran

ABSTRACT

In the current study, we proposed a facile method for fabrication of multifunctional pH- and thermo-sensitive magnetic nanocomposites (MNCs) as a theranostic agent for using in targeted drug delivery and magnetic resonance imaging (MRI). To this end, we decorated Fe_3O_4 magnetic nanoparticles (MNPs) with N,N-dimethylaminoethyl methacrylate (DMAEMA) and N-isopropylacrylamide (NIPAAm), best known for their pH- and thermo-sensitive properties, respectively. We also conjugated mesoporous silica nanoparticles (MSNs) to polymer matrix acting as drug container to enhance the drug encapsulation efficacy. Methotroxate (MTX) as a model drug was successfully loaded in MNCs (M-MNCs) *via* surface adsorption onto MSNs and electrostatic interaction between drug and carrier. The pH- and temperature-triggered release of MTX was concluded through the evaluation of *in vitro* release at both physiological and simulated tumor tissue conditions. Based on *in vitro* cytotoxicity assay results, M-MNCs significantly revealed higher antitumor activity compared to free MTX. *In vitro* MR susceptibility experiment showed that M-MNCs relatively possessed high transverse relaxivity (r_2) of about $0.15\,mM^{-1}\cdot ms^{-1}$ and a linear relationship between the transverse relaxation rate (R_2) and the Fe concentration in the M-MNCs was also demonstrated. Therefore, the designed MNCs can potentially become smart drug carrier, while they also can be promising MRI negative contrast agent.

Introduction

In recent decade, the development of nanoparticles (NPs) as controlled drug delivery and therapeutic agents has raised great interests and become one of the most promising candidates for biomedical and bioengineering applications [1–3]. Thanks to their tiny size which is far smaller than cancer cells, NPs can easily reach the diseased site and penetrate the cell barriers due to the enhanced permeability and retention (EPR) effect, which is useful in passive drug delivery systems [4]. Magnetic nanoparticles (MNPs), in particular Fe_3O_4 NPs are an important as well as exciting class of nano-scale materials which have raised extensive attention due to their potential applications in drug delivery, diagnosis, and therapy [5–7]. MNPs have great potential for targeted drug delivery (TDD) for which they can be accumulated and held in desired tissue using an external magnetic field which lets the carrier to unload its cargo at the site of action. Therefore, the exposure of healthy tissues to high toxic drugs, for example, chemotherapeutic agents and subsequently their noxious side effects would be significantly diminished [8,9]. Furthermore, preclinical and clinical trials have demonstrated them to be biocompatible

and several formulations (e.g., Combidex®, Resovist®, Endorem®, and Sinerem®) were successfully obtained FDA approval for clinical magnetic resonance imaging (MRI) and drug delivery [10–12]. In recent years, many efforts have been devoted to the design and synthesis of practical theranostic agents based on MNPs [13,14]. Rasekh et al. [15] encapsulated MNPs and a model drug into triglyceride tristearin shell using novel coaxial electrospray technique in order to obtain a theranostic agent. In a similar study, Zhang et al. [16] used tri-needle coaxial electrospraying with aim to co-encapsulation of MNPs and drug molecule within polymeric shell in order to develop an efficient complex, applicable in both therapeutic and diagnostic fields. In spite of promising results, in these studies, the superparamagnetic property of entrapped MNPs has been weakened due to being surrounded by an external layer like polymeric shells. However, a direct linkage between MNPs and polymer matrix could fix this defect. Moreover, low efficacy is one of the major challenges associated with the application of MNPs which is because of their detection and clearance by the reticuloendothelial system (RES) prior to reaching the target tissue. The variety of physicochemical properties of MNPs including size, morphology, charge, and surface chemistry directly affect their

subsequent pharmacokinetics and bio-distribution behavior and consequently alter the fate of these particles upon intravenous administration. The conjugation of hydroxyl groups at the surface of MNPS with different functional groups, silica NPs, or biocompatible stimuli-responsive polymers offers better physicochemical properties [17]. Mesoporous silica nanoparticles (MSNs), also known as excellent nano-containers, have gained many interest due to their superior properties including high structural porosity and surface area, low mass density and biocompatibility [18,19]. Moreover, because of high concentration of silanol groups at the surface of MSNs, they can easily undergo surface functionalization with various organic linkers. On the other hand, high structural porosity of MSNs provides enhanced drug-loading efficacy, so the drug molecule could be hosted within the pore channels through hydrogen bonding or electrostatic interaction [20,21]. It has been demonstrated that compared to the normal cells, the extracellular environment of a tumor tissue possesses lower pH (6.8), and even those of late endosome and lysosome are even lower (5–5.5) [17,22]. It is also reported that tumor tissue has higher temperature (40 °C) compared to the normal tissue (37 °C) [23]. These distinctive features could come in handy for fabricating multi-sensitive carriers that cleverly differentiate between healthy and tumor tissues, resulting in enhanced targeting and treatment efficacy. Among several thermo-sensitive polymers that have been developed in recent years, poly-N-isopropylacrylamide (PNIPAAm) offers great capability due to its amphiphilicity, biodegradability, large inner volume, and of course sensitivity to an external temperature stimulus [24,25]. The latter is due to the fact that PNIPAAm possesses a thermally reversible collapse behavior in higher temperatures of its lower critical solution temperatures (LCST, 32 °C), losing about 90% of its volume in aqueous environment which acts as an on–off switch for drug release [26]. The problem is, LCST of PNIPAAm is below body temperatures (37 °C), but it can be overcome by co-polymerization of PNIPAAm with other monomers [27]. On the other hand, poly-(N,N-dimethylaminoethyl methacrylate) (PDMAEMA) known as a cationic pH-sensitive polymer that can be useful from two aspects: (a) it can entrap anionic drug molecules like methotroxate (MTX) *via* electrostatic interaction, enhancing the drug-loading efficacy and (b) it can unload its cargo *via* electrostatic repulsion once the acidic condition is sensed. MTX, a common anticancer drug belonging to the antimetabolite class, possesses a similar structure to folic acid which can also act as a potential ligand for the folate receptors [28,29]. Therefore, the particles can gain access into the cancerous cells *via* receptor-mediated endocytosis (RME) [30] and release their cargo under the effect of acidic condition of endosome and lysosome. Briefly, in our designed drug carrier system, MNPs are applied as guided delivery and MRI contrast agents which were synthesized through co-precipitation method and modified by 3-(trimethoxysilyl)propyl methacrylate (TMSMA) to provide vinyl bonds at the surface of MNPs. MSNs were simply produced using Stöber technique and used as a drug container with aim of enhancing the loaded drug. PNIPAAm and PDMAEMA were used as switchable gates that determined whether the drug should be released from the carrier or not. A pH-sensitive cationic ionic liquid (CIL) was obtained by reaction between (N,N-dimethylaminoethyl methacrylate) (DMAEMA) monomers and (3-chloropropyl)trimethoxysilane. The MSNs were then decorated with CIL (CIL-MSNs) and finally, the pH- and thermo-sensitive magnetic nanocomposites (MNCs) were produced using free radical graft polymerization benefiting from vinyl bonds of CIL-MSNs, TMSMA-modified MNPs, and N-isopropylacrylamide (NIPAAm) monomers. Based on the above knowledge, we designed pH- and thermo-sensitive MNCs to encapsulate chemotherapy drug MTX and evaluated its *in vitro* drug release profile, cell cytotoxicity behavior and also we assessed its efficiency in MRI as negative contrast agent.

Materials and methods

Materials

Ferrous chloride tetrahydrate (FeCl$_2$·4H$_2$O > 99%), ferric chloride hexahydrate (FeCl$_3$·6H$_2$O > 99%), hydrochloric acid, sodium hydroxide, TMSMA (98%), and dimethyl sulfoxide (DMSO) were purchased from Sigma-Aldrich (St. Louis, MO, USA). NIPAAm (97%), DMAEMA monomers, (3-chloropropyl)trimethoxysilane, tetraethylorthosilicate (TEOS), and benzoyl peroxide (BPO) were purchased from Sigma-Aldrich (Steinem, Germany). Penicillin/streptomycin, fetal bovine serum (FBS), trypsin, RPMI1640, MTX, and all other biological reagents were purchased from Invitrogen Corporation (Carlsbad, CA, USA). All the other organic reagents were of analytical grade and purchased from Sigma-Aldrich (St. Louis, MO, USA).

Synthesis of MNPs

The MNPs were produced by a facile method based on co-precipitation of Fe^{3+} and Fe^{2+} according to the study of Wang et al. [31] with minor modifications. Briefly, FeCl$_3$·6H$_2$O (2.12 g) and FeCl$_2$·4H$_2$O (0.56 g) were added to 100 ml deionized (DI) water in a three-neck round-bottom flask. Then the solution was heated up to 95 °C and stirred vigorously under N$_2$ atmosphere for 30 min. Subsequently, 10 ml of 1 M NaOH solution was rapidly added to the above solution. After 3 h, the product was cooled to room temperature and the obtained black sediment was collected with a magnet and washed with DI water until neutral.

Modification of MNPs by TMSMA

First, a proper amount of acetic acid was added to 50 ml of ethanol (95%) solution in a round-bottom flask to adjust the pH on 4.8. Then 10 ml of TMSMA was added to the above solution and ultra-sonicated for 10 min. An adequate amount of MNPs were added to the obtained mixture and stirred for 24 h at 52 °C. Finally, the TMSMA-modified MNPs were collected, washed with ethanol, and dried under vacuum at 40 °C for 24 h.

Synthesis of MSNs

The MSNs were simply synthesized according to a modified Stöber technique [32]. The process was as follows: a mixture solution containing 1 ml of (9 M) ammonium hydroxide and 28 ml of anhydrous ethanol was prepared and stirred for 5 min at 600 rpm. Then 1 ml of TEOS was added to the above mixture rapidly and kept stirring for 24 h at ambient temperature. The obtained MSNs were precipitated with n-hexane, separated *via* centrifugation at 10,000 rpm, and consequently frozen at −80 °C and then dried under vacuum for 24 h to attain white powder.

Synthesis of pH-sensitive CIL monomer

According to the study of Salehi et al. [33], a mixture solution containing (3-chloropropyl)trimethoxysilane (6 ml) and N,N-DMAEMA (4 ml) was prepared in a three-neck round-bottom flask and stirred for 48 h at 80 °C under N$_2$ atmosphere. The product was

precipitated by the addition of dichloromethane and then we let the solvent evaporate and finally a wax-like white CIL monomer was obtained and kept at 25 °C.

Synthesis of CIL-MSNs

CIL-MSNs were prepared as follows: 250 mg of CIL monomer was completely dissolved in 30 ml DMSO by stirring for 24 h in environment temperature. Then, 1 mg MSNs was added to the above solution and kept stirring for further 48 h in same condition. The product was then obtained by centrifugation, washed three times with DI water, and finally frozen at −80 °C and then dried under vacuum for 12 h to achieve fine white powders.

Synthesis of pH- and thermo-sensitive MNCs

TMSMA-modified MNPs (100 mg), CIL-MSNs (400 mg), and NIPAAm (500 mg) were dissolved in DMSO using bath ultra-sonication for 15 min. Subsequently, 50 mg BPO (as initiator) was added to the mixture solution and the free radical polymerization was carried on in a three-neck round-bottom flask for 72 h at 80 °C under N_2 flow. The MNCs were obtained by two times centrifugation at 1000 rpm for 10 min followed by freezing at −80 °C and then drying under vacuum for 24 h. The particles were kept at 25 °C till next steps.

Drug storage

In this study, MTX was used as a model drug and the obtained carrier/drug feed ratio was 5:1. In brief, first 200 mg of freeze-dried MNCs and 40 mg MTX were dispersed in 20 ml phosphate buffer solution (PBS). The solution was stirred at 25 °C for 48 h with stirring rate of 100 rpm. The MTX-loaded MNCs (M-MNCs) were then separated from solution by external magnet and frozen at −80 °C and then dried under vacuum for 24 h. The supernatant solution was then analyzed using an ultraviolet-visible (UV-Vis) spectrophotometer (Shimadzu, Japan) to calculate the encapsulation efficiency and loading efficiency of MTX ($\lambda_{max} = 305$ nm) according to Equations (1) and (2), respectively:

$$\text{Drug encapsulation efficiency \%} = \left[\frac{\text{amount of loaded drug in mg}}{\text{amount of added drug in mg}}\right] \times 100 \tag{1}$$

$$\text{Drug loading efficiency \%} = \left[\frac{\text{amount of loaded drug in mg}}{\text{amount of added MNCs in mg}}\right] \times 100 \tag{2}$$

In vitro drug release

We assessed the drug release amount in four different conditions including pH = 7.4, 37 °C, pH = 5, 37 °C, pH = 7.4, 40 °C, and pH = 5, 40 °C. To do so, the solutions were prepared as follows: 10 mg of M-MNCs was dispersed in 2 ml of PBS with determined pH. The dispersions were then transferred into dialysis bag (molecular weight cut-off 12,000, Sigma-Aldrich, CA, USA), immersed in 28 ml of PBS as acceptor with the same pH and kept in lab shaker (Vibramix) at 120 rpm at selected temperature. At determined time intervals, 3 ml of medium was collected and the MTX absorbance was detected using UV-Vis spectrophotometer (Shimadzu, Japan) to determine the amount of released MTX ($\lambda_{max} = 305$ nm). The relative percentage of the released drug was simply calculated using Equation (3):

$$\text{Drug released \%} = \frac{\text{amount of drug in release medium in mg}}{\text{amount of drug loaded in MNCs in mg}} \times 100 \tag{3}$$

Cell culture and cell viability assay

Human lung epithelial carcinoma A549 cell line (obtained from Pharmaceutical Nanotechnology Research Center, Tabriz University of Medical Sciences, Tabriz, Iran) were cultured as described in the study of Akbarzadeh et al. [27]. Briefly, cells were cultured in Gibco® RPMI1640 supplemented with 10% (v/v) FBS, 0.05 mg ml^{-1} penicillin G, and 80 µg ml^{-1} streptomycin and incubated at 37 °C in a humidified atmosphere containing 5% CO_2 for 24 h. The MTT viability assay was applied to assess the cytotoxicity of free MTX, M-MNCs, and MNCs against A549 cells. To this end, cells were seeded in 96-well plates with a cell density of 1.0×10^4 cells/well and allowed to grow for 24 h at the same condition prior to the treatment. After cell attachment and growth resumption, cells were treated with various concentrations (25, 50, 100, 200, and 400 µg ml^{-1}) of MTX and M-MNCs and (125, 250, 500, and 1000 µg ml^{-1}) of MNCs. Control cells were added with equivalent volume of fresh media. After incubation for 48 h, the old medium of each well was replaced with 100 µl of fresh medium and 10 µl of a 5 mg ml^{-1} MTT solution and subsequently the plate was covered with aluminum foil and incubation was continued for further 4 h under cell culture conditions. Then, the unreduced MTT and old culture medium were removed and 150 µl of DMSO was added to the wells to dissolve the formazan crystals. The plate was shaken for 10 min and the absorbance was read at 570 nm with a background correction at 630 nm using an ELISA plate reader (Bio-Tek Instruments, USA) and the growth inhibition was calculated. All of the tests were performed in duplicate and statistical analyses were performed using SPSS 15 statistical software package; $p < .05$ was considered significant.

In vitro MRI study

M-MNCs were diluted with PBS to five various concentrations (0, 0.03, 0.06, 0.12, 0.25, and 0.5 mM Fe) and then added to 9-ml glass test tubes of 1 cm in diameter. T_2-weighted MRI study of the M-MNCs was accomplished using clinical 1.5 T whole-body magnetic resonance system (MAGNETOM Avanto, Siemens, Germany). Parameters for obtained multislice T_2-weighted images were as follows: multispin-echo (32 echoes), various echo times (TE) ranging from 22 ms to 352 ms, repetition time (TR) = 3500 ms, field of view (FOV) = 190 × 190 mm^2, flip angle = 180°, slice thickness = 10 mm, and point resolution = 256 × 256 mm^2. The acquired images were then processed and the magnitude of signal attenuation was extracted via manually drawn regions of interest (ROIs) using DICOM Viewer (version 5.1). Relaxivity rates R_2 ($=1/T_2$) were calculated for each concentration using the Equation (4) (S_I and S_0 stand for signal intensity and constant, respectively):

$$S_I = S_0 \times exp\left(-R_2 \times TE\right) \tag{4}$$

Characterization technique

The chemical structures of particles at each step were recorded using Fourier transform infrared spectrophotometer (FT-IR, Equniox 55 LS 101 Bruker, Germany), in which 2 mg of each

sample was mixed with 200 mg KBr and pressed to form a tablet. Infrared (IR) spectra of the samples were scanned ranging from 400 to 4000 cm^{-1} and obtained at a resolution of 4 cm^{-1} with a minimum of 256 scan per spectrum at room temperature under nitrogen gas. The spectra of KBr, CO_2, and water were subtracted from the spectrum of each sample. Elemental analysis of TMSMA-modified MNPs was performed using energy-dispersive X-ray analysis (EDX, VEGA/TESCAN, USA) and sample was prepared as the same as those for scanning electron microscope (SEM) but instead of gold, the sample was sputtered with a thin layer of carbon under vacuum prior to the elemental analysis. The EDX system was coupled with SEM using mixed BSE (back scatter electron) and LSE (lateral secondary electron) signal detectors. The mean hydrodynamic diameter, polydispersity index (PDI), and zeta potential of MNCs and M-MNCs were measured using Nano S zeta-sizer (Malvern Instruments, Malvern, UK). The samples were diluted with DI water and the mean hydrodynamic diameter (at pH = 7.4) and zeta potential (at pH = 5.8 and 7.4) analyses were repeated three times per sample at 25 °C. The magnetization curves of MNPs and MNCs were acquired using vibrating sample magnetometry (VSM, MDKFT, Meghnatis Daghigh Kavir Co., Iran) at 25 °C. Flam atomic absorption spectrometer (FAAS, novAA 400, Analytik Jena, Germany) was used to calculate the concentration of Fe embedded in the predetermined concentration of MNCs. The stock solution of 2 mg ml^{-1} was prepared in DI water and diluted 1000-fold. SEM (MIRA3/TESCAN, USA) was applied to determine the surface morphology, average diameter, and size of MNPs, MNCs, and M-MNCs. The samples were first dispersed in acetone and then a small drop of each sample was spread onto SEM locator copper grid, then it was let to be hardened and sputtered with a thin layer of gold under vacuum for 90 s. The particle size was then calculated by measuring the diameters of at least 300 particles shown in SEM using image analysis software (Image-Pro plus 4.5; Media Cybernetics, Silver Spring, MD, USA).

Result and discussion

Synthesis of pH- and thermo-sensitive M-MNCs

Figure 1 illustrates the process of synthesis of pH- and thermo-sensitive M-MNCs via a multistep procedure. In this study, we firstly synthesized the superparamagnetic MNPs through co-precipitation of Fe^{3+} and Fe^{2+} under alkali condition. Then, the surface of MNPs was modified by TMSMA via the reaction between free hydroxyl groups on the surface of MNPs and methoxy groups of TMSMA. These methoxy groups can be hydrolyzed in water and result in highly reactive silanols species which can be condensed with abovementioned hydroxyl groups. Thus, the double bands on the other end of the TMSMA provided grafting sites at the surface of MNPs which made them capable of being covalently bonded to the polymer matrix. The Stöber technique was employed for the synthesis of MSNs, in which the particles were obtained as result of hydrolysis and condensation reaction of TEOS in the presence of ammonium hydroxide [33,34]. The CIL monomer was simply synthesized through coupling of amine moiety of DMAEMA to the (3-chloropropyl)trimethoxysilane. The conjugation between MSNs and CIL monomers was performed in similar manner as explained earlier for TMSMA-modified MNPs. Again, the methoxy groups of CIL monomers were hydrolyzed in solution phase and the provided silanol groups were condensed with free surface hydroxyl groups of MSNs resulting in stable Si-O-Si bonds. Finally, the pH- and thermo-sensitive MNCs were obtained by a free radical graft polymerization benefiting from vinyl bond of CIL-MSNs, TMSMA-modified MNPs, and NIPAAm in the presence of optimally selected

concentration of initiator (BPO). It is worth noting that during the synthesis of MNCs, the MNPs and MSNs were fixed to the polymer matrix via covalent connections which prevents polymer detachment and/or leakage of MNPs and MSNs from MNCs. Two stock solutions of 2 mg ml^{-1} in PBS were made for both MNCs and M-MNCs and they were stored at 25 °C under normal condition. In 10 days, the samples showed stable behavior in physiological buffers.

Characterization

FT-IR spectroscopy of nanoparticles

The chemical structures of the MNPs, TMSMA-modified MNPs, MSNs, CIL, CIL-MSNs, and MNCs were analyzed using FT-IR spectroscopy (Figure 2). As it is shown in Figure 2(a), the strong absorption peaks at 584 cm^{-1} and 3439 cm^{-1} were related to the stretching vibration of Fe-O and free O-H groups, respectively. Compared to Figure 2(a), the new absorption peaks at 1086 cm^{-1} and 1384 cm^{-1} were appeared which are probably belong to the stretching vibration of Si-O and Si-C, respectively (Figure 2(b)). Additionally, the peaks at 1180 cm^{-1}, 1639 cm^{-1}, and 1708 cm^{-1} indicate the presence of C-O, C=C, and C=O, respectively. Furthermore, the peak at 585 cm^{-1} is due to the stretching vibration of Fe-O bonds. All these peaks imply that the TMSMA was successfully grafted to the surface of MNPs and the provided vinyl bonds were ready for further polymerization with NIPAAm and CIL-MSNs. The MSNs showed two strong peaks at 1085 cm^{-1} and 3485 cm^{-1} which are associated with the stretching vibration of Si-O and free silanol groups in MSNs, respectively (Figure 2(c)). The FT-IR spectrum of CIL contained strong peaks at 1093 cm^{-1} and 1392 cm^{-1} that are attributed to the stretching vibration of Si-O and Si-C of three methoxy silane groups, respectively (Figure 2(d)). Moreover, the stretching vibrations of C=C and C=O of esteric carbonyl of DMAEMA moiety and C-O bonds existing in methoxy groups are manifested through strong peaks at 1639 cm^{-1}, 1731 cm^{-1}, and 1273 cm^{-1}, respectively. The two strong peaks at 2775 cm^{-1} and 2972 cm^{-1} are associated with the stretching vibration of C-H (sp^3) and C-H (sp^2) groups of the aliphatic section, respectively. Compared to the FT-IR spectra of CIL, at the FT-IR spectra of CIL-MSNs (Figure 2(e)), plus all peaks related to the CIL, a strong distinctive peak was observed at 1087 cm^{-1} which is related to the stretching vibration of Si-O bonds in both MSNs and CIL. Additionally, a strong peak at 3435 cm^{-1} is attributed to the stretching vibration of free silanol groups in MSNs. The FT-IR spectrum of MNCs (Figure 2(f)) possessed absorption peaks presented at 589 cm^{-1}, 1070 cm^{-1}, 1739 cm^{-1}, and 3676 cm^{-1} that correspond to the stretching vibration of Fe-O (MNPs), Si-O (MSNs), C=O (CIL and NIPAAm), and O-H groups (MNPs and MSNs), respectively. Additionally, a weak peak at 1542 cm^{-1} is connected to the out-of-plane bending of N-H bond in NIPAAm. It is good to mention that, N-C bond usually shows absorption peak at about 1100 cm^{-1}, which is probably overlapped with the Si-O absorption peak. All the characteristic peaks of MNCs indicate the successful attachment of MNPs and MSNs onto the polymer matrix.

Magnetism test and elemental analysis

The hysteresis loops and magnetic measurement of MNPs and MNCs were illustrated in Figure 3(a). The saturation magnetization was measured to be 80.01 and 62.92 emu/g for MNPs and MNCs, respectively which proves the superparamagnetic behavior of both samples with no hysteresis effect and perfect Langevin
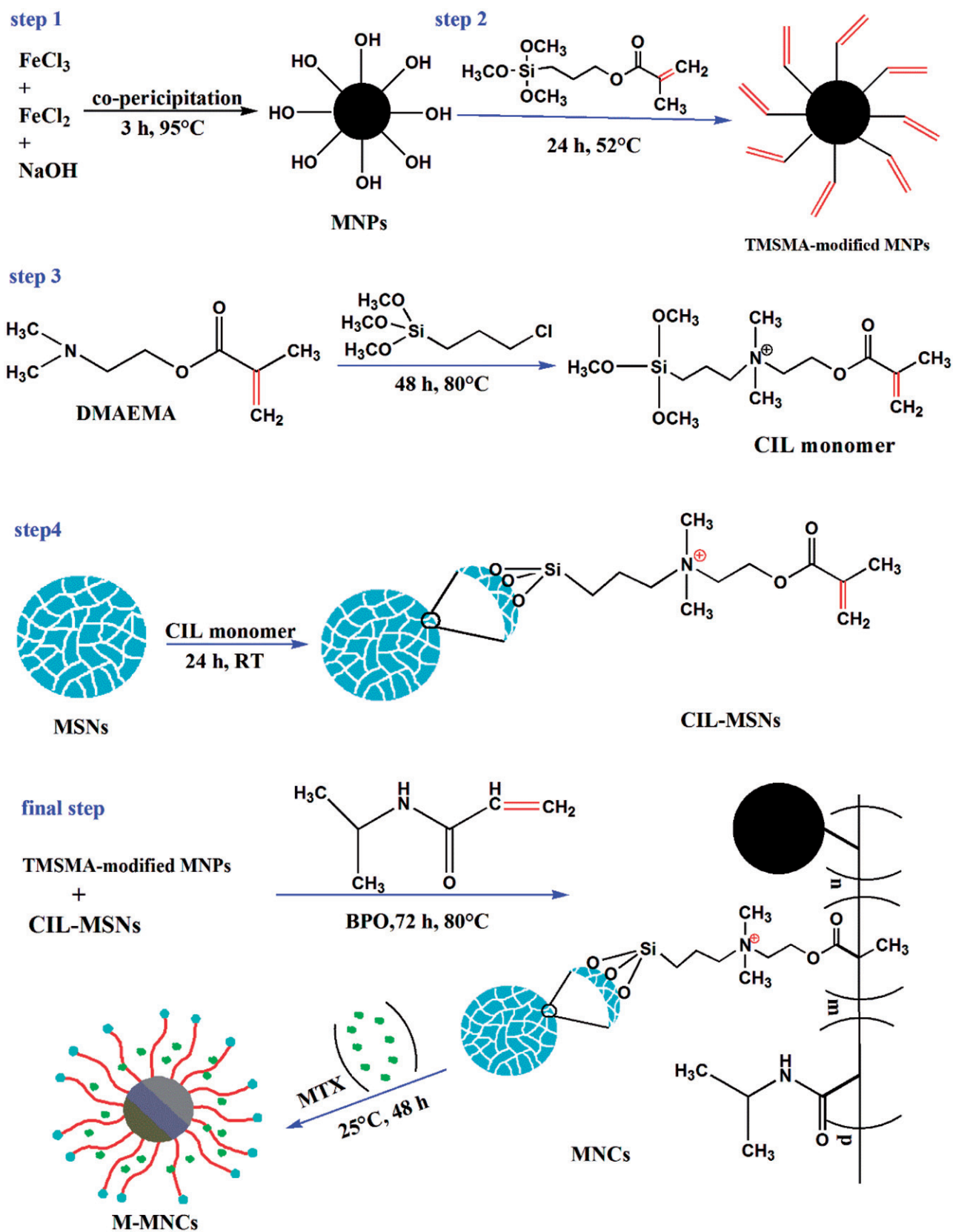
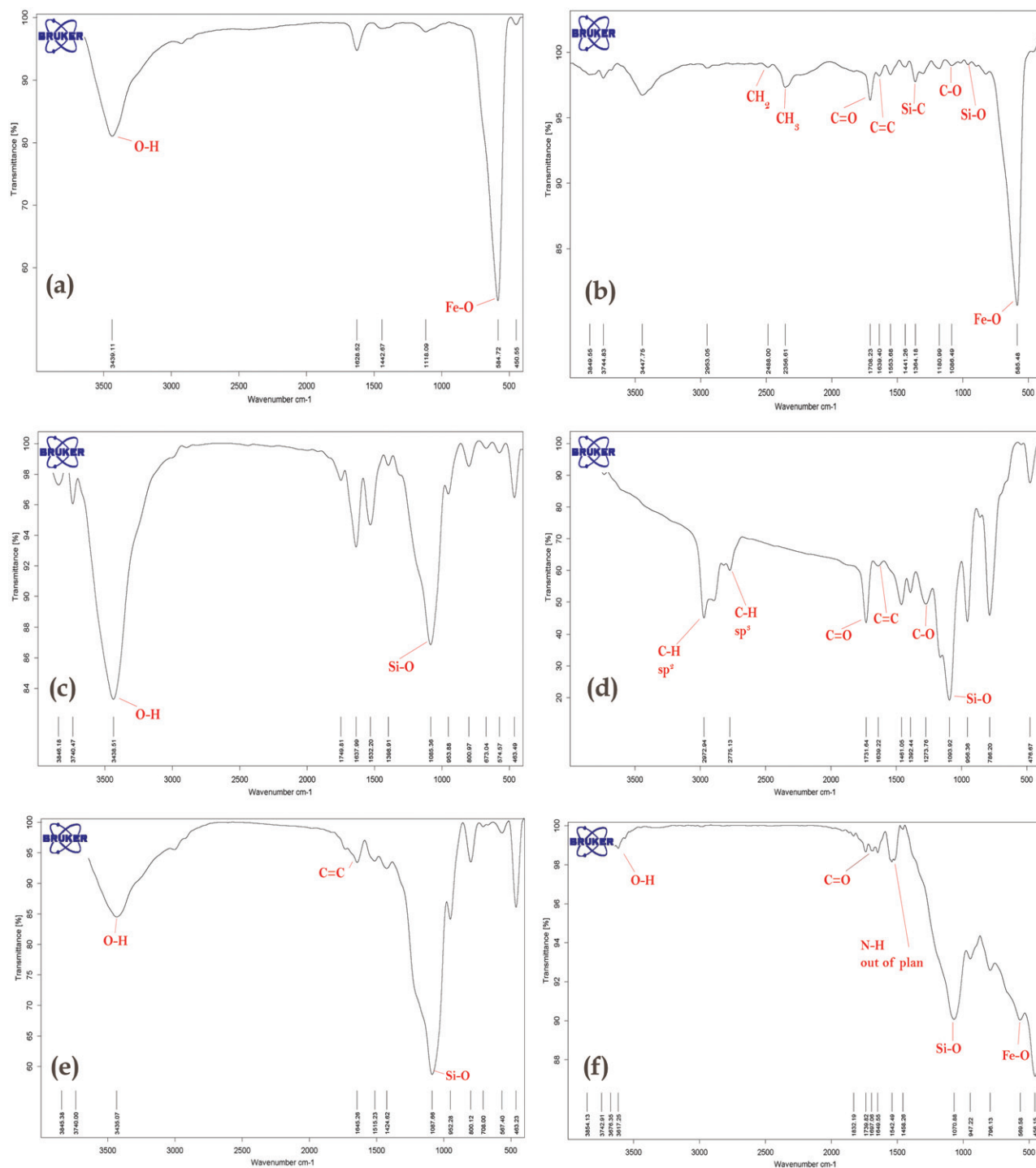Figure 1. Sequence steps in the preparation of M-MNCs.

Figure 2. FT-IR spectra of (a) MNPs, (b) TMSMA-modified MNPs, (c) MSNs, (d) CIL, (e) CIL-MSNs, and (f) MNCs.

behavior [35]. After the conjugation of MNPs to polymer matrix, the saturation magnetization was just reduced insignificantly with no remnant magnetization in the VSM curve of MNCs, which specifies that MNPs conserved their superparamagnetic characteristics in MNCs and grafting to polymer matrix had no significant effect on their magnetic properties. Superparamagnetism of MNCs indicates that they respond magnetically to an external magnetic field and by removing the magnetic field, they can be well dispersed in medium (Figure 4).

The elemental analysis of TMSMA-modified MNPs was determined by EDX spectrum (Figure 3(b)), in which the presence of Fe and O atoms in MNPs as well as Si and C (belong to TMSMA) were observed indicating that the surface of MNPs was successfully modified with TMSMA. The low percentage of Si and C atoms compared to Fe and O can be justified by the fact that there are hundreds to thousands of Fe or O atoms in the examined area, while comparatively low and limited ratio of C and Si are existing in the same area. It is also worth mentioning that the oxygenes of methoxy groups in TMSMA intensified the peak of O. The Fe concentration of $2 \, mg \, ml^{-1}$ of MNCs was measured to be $0.931 \, mg \, ml^{-1}$ (46.55%) using FAAS. This highlights the significant role of double bond of TMSMA in grafting MNPs to polymer matrix.
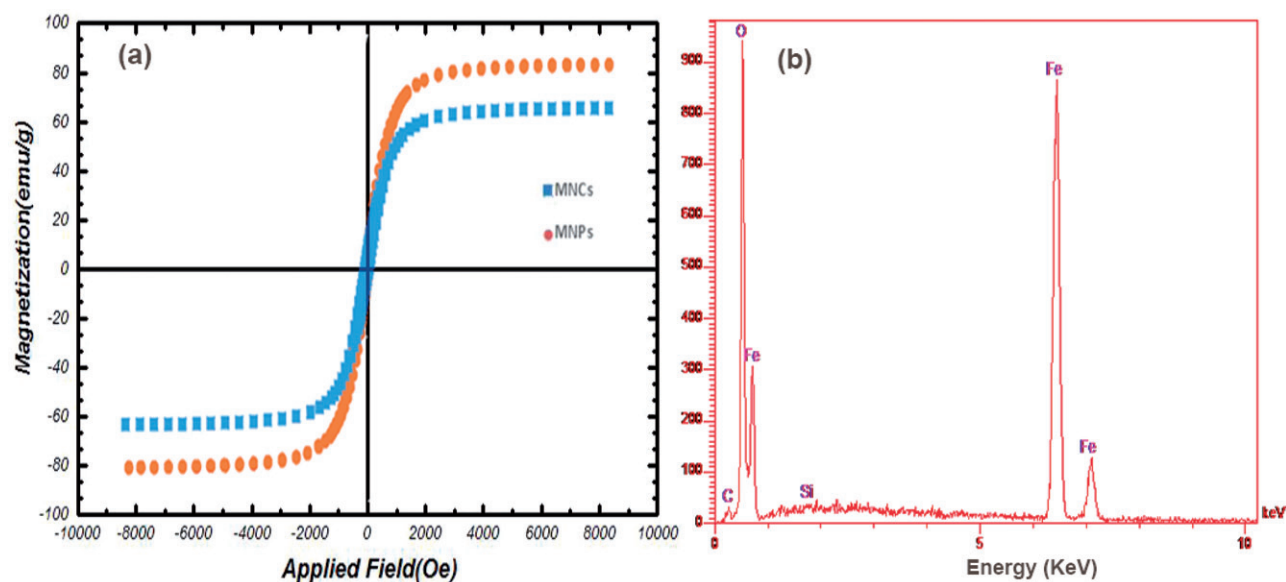
Figure 3. The magnetization curve of (a) MNPs and MNCs and (b) the EDX mapping of TMSMA-modified MNPs.
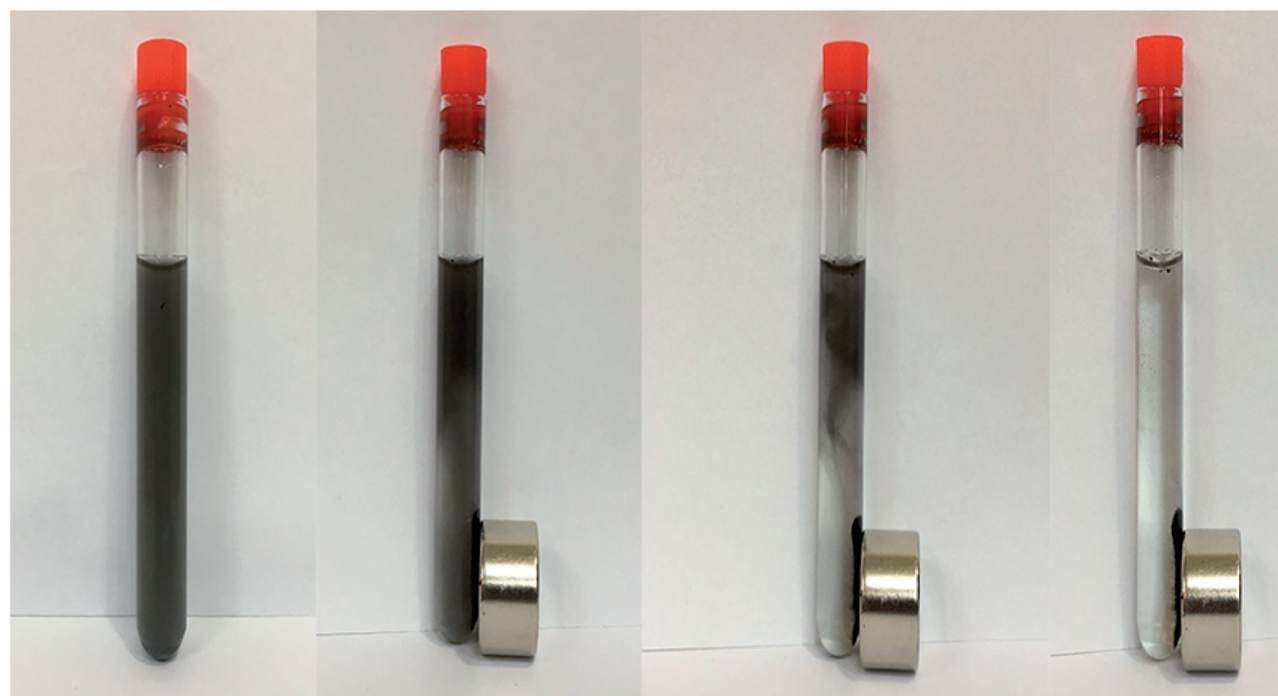

Figure 4. Magnetic response of dispersed MNCs to an external magnet (1.2 T).

Furthermore, this amount of Fe concentration was promising in following *in vitro* MRI study, which let us to work in low concentration of M-MNCs.

Hydrodynamic diameter and zeta potential

The mean hydrodynamic diameter, PDI, and zeta potential values of MNCs and M-MNCs are summarized in Table 1. As a result, at pH = 7.4, the mean diameters of MNCs and M-MNCs were 297.3 nm and 318.8 nm, respectively. Furthermore, the PDIs of MNCs and M-MNCs were measured to be 0.3 and 0.6, respectively,

which indicates the mid-range polydispersity of both samples. At pH = 7.4, the MNCs and M-MNCs showed negative zeta potential of −7.51 mV and −22.4 mV, respectively, which was expected due to ionization of surface hydroxyl groups at the surface of MNPs (pKa 6.8) [36] and turning into ionized form (-O⁻) that caused negative zeta potential. Moreover, the additional -COO⁻ groups in MTX (pKa 4.9 and 5.6) [33] are probably responsible for lower zeta potential of M-MNCs compared to MNCs. By decreasing the pH to 5, the zeta potential increased to +2.02 mV and +16.8 mV, for MNCs and M-MNCs, respectively. At this pH, the abovementioned -O⁻ groups were protonated that accompanying with the cationic

amino moiety of DMAEMA in MNCs, increased the zeta potential in both samples. Additionally, we witnessed a higher zeta potential for M-MNCs compared to MNCs, which is because of the further protonation of amine groups ($-NH_3^+$) existing in MTX. All these results prove the pH-sensitive properties of MNCs.

Size and morphology

The size and morphology of MNPs, MNCs, and M-MNCs were obtained using SEM (Figure 5). Based on results, the uniformity in size and shape of particles were revealed on which the average size of MNPs, MNCs, and M-MNCs were about 20, 51, and 62 nm, respectively. These sizes are perfectly within the desired range of the NPs useful for effective drug delivery [37]. Figure 5(a) shows that there was aggregation with MNPs which is common phenomena for bare MNPs and they tend to precipitate and aggregate which is observed in other studies [27,38]. After grafting to the polymer matrix, owing to positive charge on polymer chains and electrostatic repulsion among them, the dispersion of particles was moderately improved in MNCs and M-MNCs (Figure 5(b,c)).

Drug loading and release experiments

As the structure of designed MNCs in this study was not core-shell, we sought for a solution to enhance the MTX-loading amount within MNCs. Therefore, we utilized the strong adsorption ability of MSNs, for which they acted as a container for MTX and entrapped the drug molecule within their porous structures. At pH 7.4, the surface adsorption can be occurred through hydrogen bonding between the surface-hydroxyl groups (-OH) in MSNs and amino groups ($-NH_2$) existing in chemical structure of MTX (pKa

4.9 and 5.6). Furthermore, at this pH, due to $-COO^-$ groups in MTX, the net charge of MTX is negative which results in an electrostatic attraction between MTX and the cationic amino moiety of DMAEMA. The encapsulation efficiency and loading efficiency of MTX were calculated to be 68% and 13.6%. The low loading efficiency value is due the fact that the carrier/drug feed ratio was 5:1 and according to Equation (2), the maximum loading efficiency could be 20% at the ideal condition. The drug release performances of pH- and thermo-sensitive M-MNCs were evaluated at the pH values of 7.4 and 5 and different temperatures of 37 °C and 40 °C for 125 h (~5 days). As illustrated in Figure 6, only 38.8% of MTX was released at pH 7.4 and 37 °C which indicates the poor release of MTX in physiological conditions. When the pH dropped to 5 which is below the pKa of MTX, the MTX released amount reached to 59%. This result can be attributed to the fact that, at this pH the abovementioned anionic carboxylate groups ($-COO^-$) in MTX were gradually protonated. In the meantime, the amino groups ($-NH_2$) of MTX were protonated and resulted in cationic $-NH_3^+$. As a result, the electrostatic repulsion between these cationic groups and the cationic amino moiety of DMAEMA could result in the enhancement of drug release from carrier which shows pH-sensitive release behavior of carrier. To confirm the significant role of PNIPAAm as a thermo-sensitive polymer in drug

Table 1. Mean hydrodynamic diameter, PDI, and zeta potential of MNCs and M-MNCs.

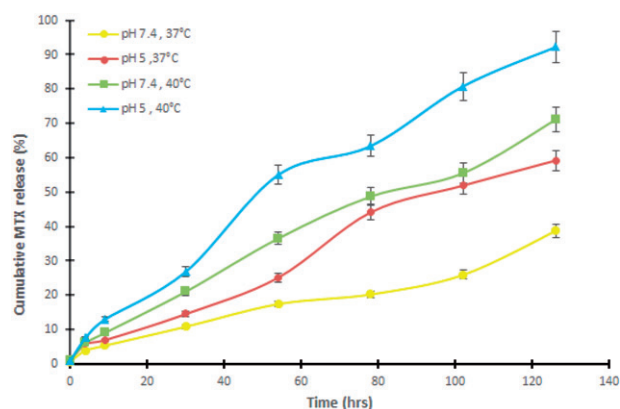|	Size (nm)	PDI	Zeta potential (mV) (pH 7.4)	Zeta potential (mV) (pH 5)
MNCs	297.3	0.3	−7.51	+2.02
M-MNCs	318.8	0.6	−22.4	+16.8

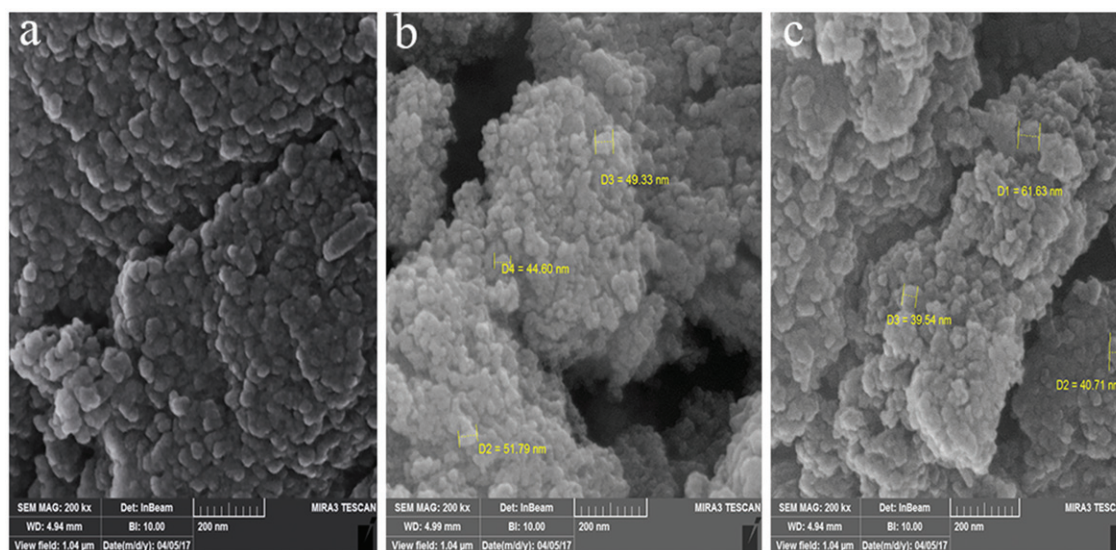**Figure 6.** Cumulative *in vitro* release profile of MTX at different conditions.

Figure 5. SEM images of (a) MNPs, (b) MNCs, and (c) M-MNCs.

release, we increased the temperature up to 40 °C above the LCST of PNIPAAm (37 °C) at pH 7.4. The drug released amount reached to 71.2% within 5 days. This can be explained by the fact that, at temperatures above the LCST of PNIPAAm, the polymer undergoes a phase transition and the hydrogen bonds between the water and polymer break which causes a collapse in polymer shell, shrink in the mesh size of gel, and consequently release of loaded drug. This is why 32.4% of more MTX was released from M-MNCs compared to the release profile at 37 °C (38.8%) during 5 days.

Finally, we assessed the MTX released amount in the simulated tumor tissue conditions which was meant to be at pH 5 and 40 °C. Excitingly, the released amount was highest (92.3%) especially compared to the physiological conditions (38.8%), which was most likely due to the combination of pH- and thermo-sensitive properties of designed nanocarriers. All these results introduce the MNCs as a gatekeepers which effectively prevent the release of drug in physiological conditions, while they release their maximum cargo in environment which is most similar to the tumor tissue conditions.

In vitro *cell viability assay*

Using A549 cell line as an *in vitro* cell model, therapeutic efficacy of M-MNCs was evaluated compared to free MTX by MTT viability assay for 48 h. The study was performed at various concentrations of MTX ranging from 25 to 400 μg ml^{-1}. As depicted in Figure 7, after 48 h, the M-MNCs meaningfully showed higher dose-dependent cell cytotoxicity compared to free MTX. This could be related to the fact that the free drug is quickly refluxed out of the cell by p-glycoproteins, whereas the M-MNCs can internalize into cells through one-way RME and gradually release the drug molecule as a result of harsh acidic condition [21] within cell which is discussed earlier. The half-maximal inhibitory concentration (IC$_{50}$) values were 374 and 663.3 μg ml^{-1} for M-MNCs and free MTX, respectively, which significantly indicates higher antitumor activity of M-MNCs than free MTX. We also evaluated the cytotoxicity effect of drug-free MNCs at different concentrations against A549 cell line (Figure 7). Based on results, no significant cytotoxicity was reported compared to negative control up to concentration of 1000 μg ml^{-1} of MNCs which proves the biocompatibility of designed MNCs. It must be emphasized that, at higher concentrations of MNCs (>5882 μg ml^{-1}) the cell viability percentage dropped to 65%, indicating that MNCs alone can show cytotoxic behavior at higher concentrations which are of course far beyond required concentration for MNCs to show therapeutic efficacy. We assume that the designed carriers could be more valuable *in vivo* studies not only due to passive tumor targeting through their EPR effect, but also because of their TDD capability under external magnetic field relying on the superparamagnetic properties of MNCs which is proved earlier. Therefore, the particles can accumulate in desired tissue that results in the reducing of required drug dosage as well as undesired drug side effects.

In vitro *MRI experiment*

By dephasing transverse magnetization and lowering the value of transverse relaxation time T$_2$, MNPs are known as a famous T$_2$-weghted negative contrast agent. Therefore, we were meant to determine relaxation time and MRI proficiency of M-MNCs at various concentrations of Fe (0, 0.03, 0.06, 0.12, 0.2, and 0.5 mM) using 1.5 T MRI system. Based on results, the more Fe concentration
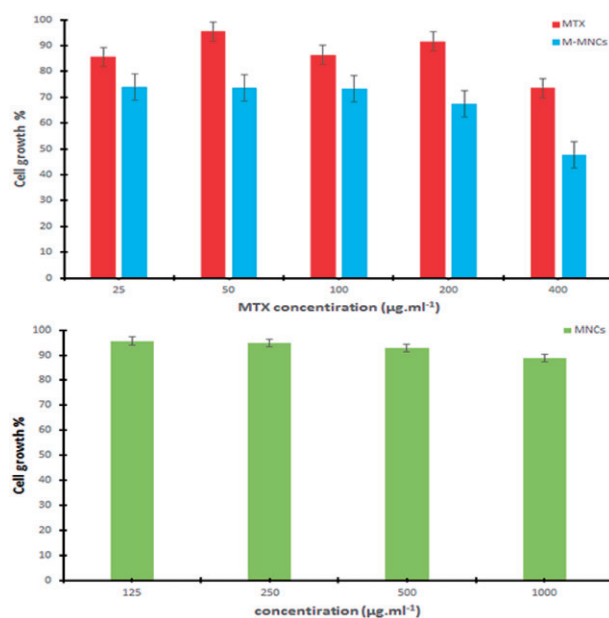

Figure 7. Cell growth inhibition rates by different concentration of free MTX, M-MNCs, and MNCs against lung cancer (A549) cell line for 48 h.

enhanced in M-MNCs, the weaker T$_2$ signal intensity became and higher contrast in MRI images was observed (Figure 8(a,b)). The plot of the relaxation rate, R2 (=1/T2), of M-MNCs as a function of Fe concentration is illustrated in Figure 8(c). It can be seen that the R$_2$ was linearly fitted to the Fe concentrations in which the T$_2$ intensity significantly decreased from 161.29 to 13.1 ms. Furthermore, the T$_2$ relaxivities (r$_2$) value of M-MNCs which is the slope of plot, calculated to be 0.15 mM^{-1} ms^{-1} which is as high as pure MNPs reported in similar studies [39,40]. These results suggest that the MNPs in M-MNCs preserved their superparamagnetic properties offering M-MNCs as promising T$_2$-weghted contrast agent in MRI.

Conclusions

In this study, we developed a new pH- and thermo-sensitive nanocomposites based on MNPs as a theranostic agent. The MNPs were modified with TMSMA which created reactive vinyl groups at the surface of MNPs. Therefore, CIL-MSNs and NIPAAm were bonded to MNPs *via* radical polymerization resulting in pH- and thermo-sensitive MNCs. MNPs kept their superparamagnetic properties after grafting to the polymer matrix. Surface adsorption onto MSNs and electrostatic interaction between positive charge of carrier and negative charge of MTX were two strategies used to entrap the drug molecules within MNCs. Based on *in vitro* release results, the designed carrier acted as a gatekeeper that meaningfully prevented the drug release at physiological conditions (condition existing in normal tissue), whereas by reducing the pH and increasing the temperature (simulating tumor tissue surroundings) the drug release amount was significantly increased indicating pH- and thermo-sensitive behavior of MNCs. The *in vitro* cellular cytotoxicity study showed that the MNCs are biocompatible and had no cytotoxic effect on A549 cell line in required concentrations. However, negligible cytotoxic behavior of MNCs was reported at higher concentrations. In addition, the M-MNCs demonstrated promising dose-dependent anticancer efficacy against A548 cell which was completely incomparable with the weak effect of free MTX in equal concentrations. Furthermore, *in vitro* T$_2$ relaxometry
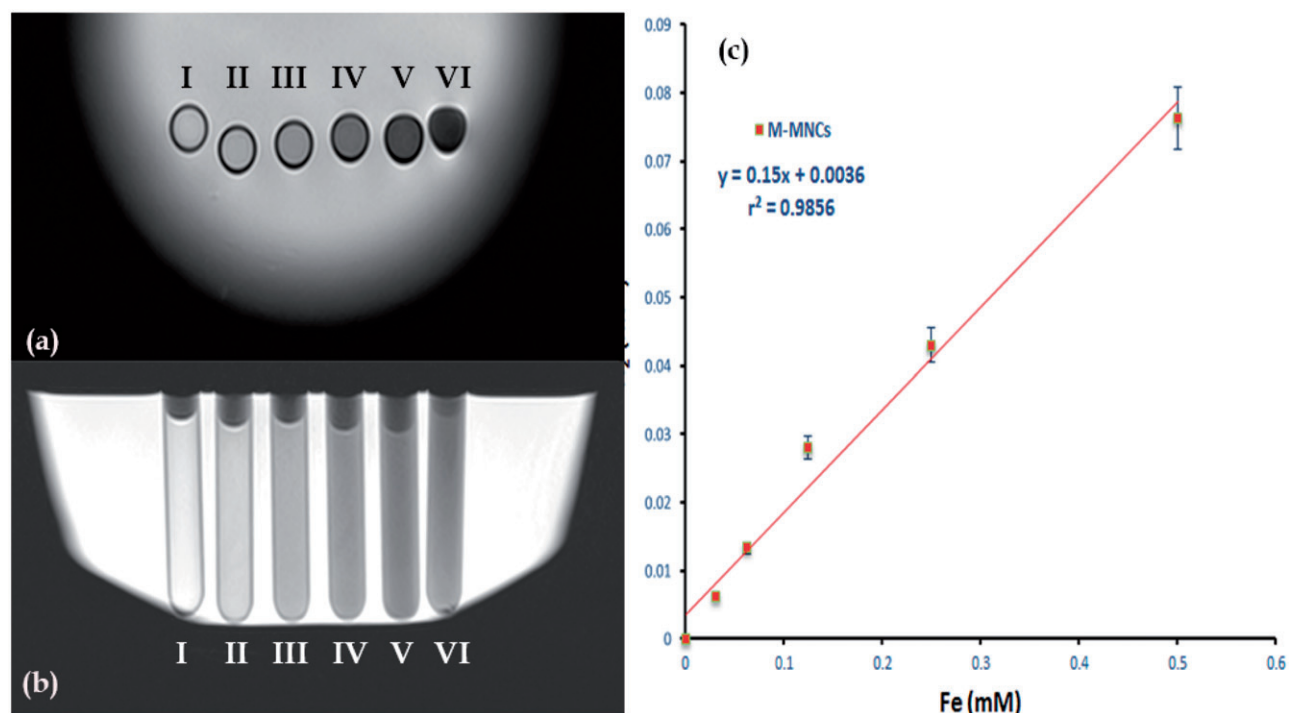
Figure 8. The *in vitro* MRI images using 1.5 T scanner (TR = 3500 ms; TE = 22 ms) are shown in (a) top view and (b) side view. M-MNCs were used at different concentrations of Fe (I–VI are 0, 0.03, 0.06, 0.12, 0.2, and 0.5 mM, respectively). (c) T_2 relaxation rate (R_2) of M-MNCs versus Fe concentration. Note: Data as values obtained from curve fitting.

measurement showed that the obtained M-MNCs have relaxivity of $0.15\,mM^{-1}\,ms^{-1}$ which offers their employment as a T_2-weghted negative contrast agent for MRI. In conclusion, we can claim that the pH- and thermo-sensitive M-MNCs may have the potential to be promising theranostic agent to serve as both targeted anticancer drug carrier and MRI contrast agent for lung cancer patients.

Disclosure statement

The authors declare that they have no competing interests. The authors alone are responsible for the content and writing of this article.

References

[1] Shakoori Z, Ghanbari H, Omidi Y, et al. Fluorescent multi-responsive cross-linked P(N-isopropylacrylamide)-based nanocomposites for cisplatin delivery. Drug Dev Indus Pharm. 2017;43:1283–1291.

[2] Panahi Y, Farshbaf M, Mohammadhosseini M, et al. Recent advances on liposomal nanoparticles: synthesis, characterization and biomedical applications. Artif Cells Nanomed Biotechnol. 2017;45:788–799.

[3] PanahiMohammadhosseini Y, Nejati-Koshki MK, Abadi AJN, et al. Preparation, surface properties, and therapeutic applications of gold nanoparticles in biomedicine. Drug Res. 2017;67:77–87.

[4] Prabhakar U, Maeda H, Jain RK, et al., Challenges and key considerations of the enhanced permeability and retention effect for nanomedicine drug delivery in oncology. Cancer Res. 2013;73:2412–2417.

[5] Shao H, Min C, Issadore D, et al. Magnetic nanoparticles and microNMR for diagnostic applications. Theranostics. 2012;2:55–65.

[6] Schotter J, Schrittwieser S, Muellner P, et al. Optical biosensor technologies for molecular diagnostics at the point-of-care. SPIE Sens Technol + Appl. 2015;10.

[7] Lian Q, Zheng X. Synthesis and application of magnetic chitosan nanoparticles in oilfield. Russ J Phys Chem. 2016;90:158–165.

[8] Shabestari Khiabani S, Farshbaf M, Akbarzadeh A, et al. Magnetic nanoparticles: preparation methods, applications in cancer diagnosis and cancer therapy. Artif Cells Nanomed Biotechnol. 2017;45:6–17.

[9] Ye F, Barrefelt Å, Asem H, et al. Biodegradable polymeric vesicles containing magnetic nanoparticles, quantum dots and anticancer drugs for drug delivery and imaging. Biomaterials. 2014;35:3885–3894.

[10] Vo-Dinh T. Nanotechnology in biology and medicine: methods, devices, and applications. Boca Raton, London, New York: Taylor & Francis Group, CRC Press, 2007.

[11] Mou X, Ali Z, Li S, et al. Applications of magnetic nanoparticles in targeted drug delivery system. J Nanosci Nanotechnol. 2015;15:54–62.

[12] Ulbrich K, Holá K, Šubr V, et al. Targeted drug delivery with polymers and magnetic nanoparticles: covalent and noncovalent approaches, release control, and clinical studies. Chem Rev. 2016;116:5338–5431.

[13] Yapa AS, Bossmann SH. Development of magnetic theranostic agents. Magn Nanomater. 2017;172–194.

[14] Kang T, Li F, Baik S, et al. Surface design of magnetic nanoparticles for stimuli-responsive cancer imaging and therapy. Biomaterials. 2017;136:98–114.

[15] Rasekh M, Ahmad Z, Cross R, et al. Facile preparation of drug-loaded tristearin encapsulated superparamagnetic iron oxide nanoparticles using coaxial electrospray processing. Mol Pharm. 2017;14:2010–2023.

[16] Hafeli U, Schutt W, Teller J, et al. Scientific and clinical applications of magnetic carriers. New York: Springer Science & Business Media, Plenum Press; 2013.

[17] Sahoo B, Devi KSP, Banerjee R, et al. Thermal and pH responsive polymer-tethered multifunctional magnetic nanoparticles for targeted delivery of anticancer drug. ACS Appl Mater Interfaces. 2013;5:3884–3893.

[18] Zheng H, Huang Z, Che S. Mesostructured chitosan–silica hybrid as a biodegradable carrier for a pH-responsive drug delivery system. Dalton Trans. 2012;41:5038–5044.

[19] Tang D, Liu B, Niessner R, et al. Target-induced displacement reaction accompanying cargo release from magnetic mesoporous silica nanocontainers for fluorescence immunoassay. Anal Chem. 2013;85:10589–10596.

[20] Youssef NA, Gurbanov EM, Haciyeva SR, et al. Antioxidant enzymes, fluctuating asymmetry and morphological changes of urban trees as an ecological indicator of heavy metal stress. Int J Pharm Sci Health Care. 2013;1:1–18.

[21] Kwon S, Singh RK, Perez RA, et al. Silica-based mesoporous nanoparticles for controlled drug delivery. J Tissue Eng. 2013;4:2041731413503357.

[22] Sun H, Guo B, Li X, et al. Shell-sheddable micelles based on dextran-SS-poly (ε-caprolactone) diblock copolymer for efficient intracellular release of doxorubicin. Biomacromolecules. 2010;11:848–854.

[23] Dai Z. Advances in nanotheranostics II: cancer theranostic nanomedicine. Vol. 7. Singapore, Heidelberg, New York, Dordrecht, London: Springer; 2016.

[24] Zhang H, Niu Q, Wang N, et al. Thermo-sensitive drug controlled release PLA core/PNIPAM shell fibers fabricated using a combination of electrospinning and UV photo-polymerization. Eur Polym J. 2015;71:440–450.

[25] Yu H, Jia Y, Chen G, et al. Fabrication of core/sheath PCL/PEG–PNIPAAm fibers as thermosensitive release carriers by a new technique combining blend electrospinning and ultraviolet-induced graft polymerization. Mater Lett. 2016;164:505–508.

[26] Zhang F, Wu W, Zhang X, et al. Temperature-sensitive poly-NIPAm modified cellulose nanofibril cryogel microspheres for controlled drug release. Cellulose. 2016;23:415–425.

[27] Akbarzadeh A, Samiei M, Joo SW, et al. Synthesis, characterization and in vitro studies of doxorubicin-loaded magnetic nanoparticles grafted to smart copolymers on A549 lung cancer cell line. J Nanobiotechnol. 2012;10:46.

[28] Chen J, Huang L, Lai H, et al. Methotrexate-loaded PEGylated chitosan nanoparticles: synthesis, characterization, and in vitro and in vivo antitumoral activity. Mol Pharm. 2013;11:2213–2223.

[29] Rosenholm JM, Peuhu E, Bate-Eya LT, et al. Cancer-cell-specific induction of apoptosis using mesoporous silica nanoparticles as drug-delivery vectors. Small. 2010;6:1234–1241.

[30] Rahimi M, Safa KD, Alizadeh E, et al. Dendritic chitosan as a magnetic and biocompatible nanocarrier for the simultaneous delivery of doxorubicin and methotrexate to MCF-7 cell line. New J Chem. 2017;41:3177–3189.

[31] Wang X, Ding X, Zheng Z, et al. Magnetic molecularly imprinted polymer particles synthesized by suspension polymerization in silicone oil. Macromol Rapid Commun. 2006;27:1180–1184.

[32] Muriithi B, Loy D. Proton conductivity of nafion/ex-situ sulfonic acid-modified Stöber silica nanocomposite membranes as a function of temperature, silica particles size and surface modification. Membranes. 2016;6:12.

[33] Salehi R, Hamishehkar H, Eskandani M, et al. Development of dual responsive nanocomposite for simultaneous delivery of anticancer drugs. J Drug Target. 2014;22:327–342.

[34] Muriithi B, Loy DA. Processing, morphology, and water uptake of nafion/ex situ stober silica nanocomposite membranes as a function of particle size ACS Appl Mater Interfaces. 2012;4:6766–6773.

[35] Chen Z, Zhang Y, Zhang S, et al. Preparation and characterization of water-soluble monodisperse magnetic iron oxide nanoparticles via surface double-exchange with DMSA. Colloids Surfaces A Physicochem Eng Asp. 2008;316:210–216.

[36] Lamanna G, Kueny-Stotz M, Mamlouk-Chaouachi H, et al. Dendronized iron oxide nanoparticles for multimodal imaging. Biomaterials. 2011;32:8562–8573.

[37] Faraji AH, Wipf P. Nanoparticles in cellular drug delivery. Bioorg Med Chem. 2009;17:2950–2962.

[38] Rahimi M, Shojaei S, Safa KD, et al. Biocompatible magnetic tris (2-aminoethyl) amine functionalized nanocrystalline cellulose as a novel nanocarrier for anticancer drug delivery of methotrexate. New J Chem. 2017;41:2160–2168.

[39] Deng L, Ke X, He Z, et al. A MSLN-targeted multifunctional nanoimmunoliposome for MRI and targeting therapy in pancreatic cancer. Int J Nanomedicine. 2012;7:5053–5065.

[40] Cai H, Li K, Shen M, et al. Facile assembly of Fe_3O_4@Au nanocomposite particles for dual mode magnetic resonance and computed tomography imaging applications. J Mater Chem. 2012;22:15110–15120.